ACS APPLIED ENERGY MATERIALS

Subscriber access provided by - Access paid by the | UCSB Libraries

Article

Zinc as new dopant for NiOx based planar perovskite solar cells with stable efficiency near 20%

Xingxing Wan, Yanan Jiang, Zhiwen Qiu, Hailiang Zhang, Xiaomeng Zhu, Iqbal Sikandar, xiaobin liu, Xin Chen, and Bingqiang Cao

ACS Appl. Energy Mater., **Just Accepted Manuscript** • Publication Date (Web): 09 Jul 2018

Downloaded from http://pubs.acs.org on July 9, 2018

Just Accepted

"Just Accepted" manuscripts have been peer-reviewed and accepted for publication. They are posted online prior to technical editing, formatting for publication and author proofing. The American Chemical Society provides "Just Accepted" as a service to the research community to expedite the dissemination of scientific material as soon as possible after acceptance. "Just Accepted" manuscripts appear in full in PDF format accompanied by an HTML abstract. "Just Accepted" manuscripts have been fully peer reviewed, but should not be considered the official version of record. They are citable by the Digital Object Identifier (DOI®). "Just Accepted" is an optional service offered to authors. Therefore, the "Just Accepted" Web site may not include all articles that will be published in the journal. After a manuscript is technically edited and formatted, it will be removed from the "Just Accepted" Web site and published as an ASAP article. Note that technical editing may introduce minor changes to the manuscript text and/or graphics which could affect content, and all legal disclaimers and ethical guidelines that apply to the journal pertain. ACS cannot be held responsible for errors or consequences arising from the use of information contained in these "Just Accepted" manuscripts.

ACS Publications

is published by the American Chemical Society. 1155 Sixteenth Street N.W., Washington, DC 20036

Published by American Chemical Society. Copyright © American Chemical Society. However, no copyright claim is made to original U.S. Government works, or works produced by employees of any Commonwealth realm Crown government in the course of their duties.

Zinc as a New Dopant for NiO_x based Planar Perovskite Solar Cells with Stable Efficiency near 20%

Xingxing Wan[a], Yanan Jiang[a], Zhiwen Qiu[a], Hailiang Zhang[a], Xiaomeng Zhu[a], Iqbal Sikandar[a], Xiaobing Liu[b], Xin Chen[b*] , Bingqiang Cao[a, b*]

[a] Materials Research Center for Energy and Photoelectrochemical Conversion, School of Material Science and Engineering, University of Jinan, Jinan 250022, Shandong, China.

[b] School of Physics and Physical Engineering, Shandong Provincial Key Laboratory of Laser Polarization and Information Technology, Qufu Normal University, 273165, Qufu, China.

[*] Corresponding Email:
mse_caobq@ujn.edu.cn or chenxin@qfnu.edu.cn.

Abstract

Organic-inorganic lead halide perovskite solar cells are potential alternatives to commercial silicon solar cells due to the attractive photon conversion efficiency and general material costs except the widely adopted organic hole transporting polymers which are currently expensive and have low conductivity. Inorganic hole transporting layer (HTL) have recently garnered attention due to their excellent stability and relatively effective cost. Nickel oxide (NiO_x) is a typical p-type oxide semiconductor with deep valance band (VB) and expected to be used as HTL. Unfortunately, the charge extraction efficiency has been hindered by its poor conductivity, resulting in lower efficiency when compared with organic HTLs based devices. Here, we report a new solution-processed doping strategy for NiO_x with zinc dopant to improve its conductivity for perovskite solar cells. The NiO_x:Zn HTL showed high transparency and significantly enhanced electrical conductivity in comparation with the pristine NiO_x. Our best NiO_x:Zn-based P-i-N planar device showed an efficiency of 19.6% with negligible hysteresis, which is comparable with the reported planar solar cell with organic HTL. Moreover, the NiO_x:Zn based perovskite device displayed distinguished stability in ambient conditions. This paper demonstrated important progress towards high-efficiency planar perovskite devices with low-cost inorganic HTLs.

Keywords: inverted planar structure, zinc dopant, hole extraction layer, high efficiency, perovskite solar cell

1. Introduction

Organic-inorganic halide perovskites solar cells with very high power conversion efficiency (PCE) up to 22% was realized only in few past years since its discovery in 2009.[1] Their intriguing optoelectronic properties, e.g. direct and tunable band gap, low exciton binding energy, long carrier diffusion length, broad absorption range,[2-7] and cost-effective processing have triggered the rapid advances in thin film solar cells.[8] Planar structures for hybrid perovskite solar cells have recently attracted much attention, due to their simple and low-cost device fabrication processing. The hole extraction/transport layers are crucial to planar perovskite solar cells (PSCs), and tremendous efforts were devoted to optimize selective charge extraction layers for enhancing photocarriers extraction efficiency and reducing charge recombination at the surfaces.[9-13] The organic hole-transporting layers (HTL), including PEDOT:PSS,[14,15] PTAA,[16] Spiro-OMeTAD[17,18] have commonly used in the planar PSCs. However, the high price and poor stability of the organic HTLs impede the development of perovskite photovoltaic toward industrial technology.[19,20] In contrast to organic HTLs, the inorganic HTLs like CuSCN,[21,22] CuI,[23] CuO,[24] and NiO_x[25-29] demonstrate superior stability, lower cost and much higher carrier mobility. As most promising candidate, NiO_x interlayer endorses numerous merits such as intrinsic p-type conductivity, high transmittance, and deep valence band (VB of 5.4 eV) that matches well with the VB of $CH_3NH_3PbI_3$.[30,31] However, the undesired conductivity and poor crystallinity of NiO_x impedes the further development on improving the performance for PSCs, which results in increased recombination rate and reduced hole

extraction efficiency.[32]

It is particularly to note that increasing the conductivity of wide bandgap metal oxide semiconductors like n-type ZnO and p-type NiO by doping is challenging as there exists a fundamental asymmetry with respect to the dopability by donors or acceptors. NiO_x is a prototype p-type wide bandgap semiconductor with rather low intrinsic conductivity (~ 10^{-13} S cm^{-1}).[33] The p-type conductivity of NiO_x is intimately connected to concentration of Ni vacancies, which arise from the composition nonstoichiometry because of the existence of a higher oxidation state of Ni^{3+} in Ni_2O_3 in NiO matrix. Doping NiO_x with metal ions like Cu, Li, Cs lowers the ionization energy of the Ni vacancies and thereafter improves the hole conductivity in NiO_x films.[34-36]

Recently, considerable attention has been devoted to the metal ion doped NiO_x film, aiming to replace the organic HTL for high efficiency PSCs. Yao *et al*.[37] applied a composite NiO_x:Cu HTL that can collect charges efficiently at the NiO_x/perovskite interface and minimize interfacial recombination . Moreover, Li doping with pulsed laser deposition (PLD) to reduce the resistivity of NiO_x films has been reported by our group,[38] which affords a powerful growth technique for thin films to tune the crystalline and physical properties. Furthermore, Chen *et al.*[39] selected the NiO_x:Cs films as a hole extraction layer to achieve a memorable device efficiency. However, these works does not discuss the physical origin of the device performance and the doping effect on the implication of Ni vacancies for the creation of free carriers also remains unknown.

In this study, we introduce zinc (Zn) doping strategy to improve the p-type conductivity of NiO_x for high-efficiency inverted planar PSCs and address the mechanism of conductivity enhancement by Zn doping which is supported by density functional theory (DFT) simulations. The NiO_x:Zn films exhibit morphology uniformity, high transparence, enhanced conductivity, and reliable reproducibility, which facilitate the high performance inverted planar PSCs with efficiency of 19.6%. Moreover, the PSCs based on NiO_x:Zn showed decent stability, with 90% of original efficiency after 720 hrs of storage in ambient conditions. This result provides a highly promising route to realize high efficiency and stable inverted planar PSCs using abundant low cost inorganic HTLs.

2. Results and Discussions

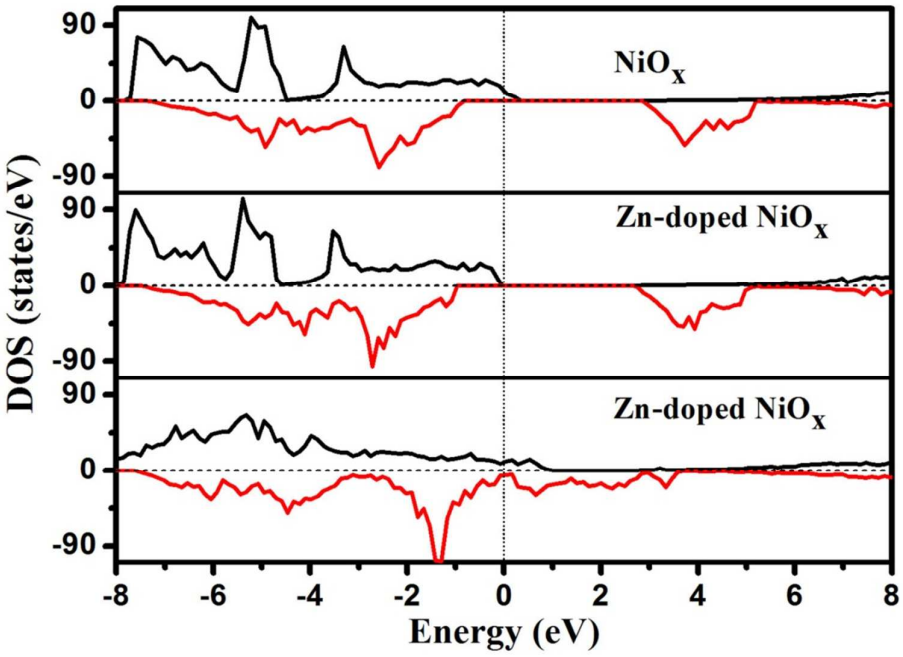

Figure 1. Spin-decomposed density of states of a 2 × 2 × 2 NiO_x supercell with a Ni vacancy (the top panel), with one Ni atom replaced by a Zn atom (the middle panel), and the supercell containing a Ni vacancy plus a substituted Zn atom (the bottom panel). Zero energy is set at the Fermi level . Positive and negative scale corresponds to the spin-up and spin-down components, respectively.

Doping is an effective method to tune the electrical attributes of semiconductors. In this work, Zn is selected as a dopant as it has a similar atomic radius 134 pm with Ni atom 125 pm, which will facilitate the incorporation of the dopant into the NiO_x matrix lattice. To deeply understand the effects of Zn doping on the electronic structures of NiO_x, we checked the electronic density of states of three supercell systems: (a) with a Ni vacancy by removing a Ni atom ($Ni_{31}O_{32}$), (b) with a Zn atom replaced by a Ni atom ($ZnNi_{31}O_{32}$), and (c) having both a Ni vacancy and a substituted Zn atom ($ZnNi_{30}O_{32}$). It is clearly seen from the spin-decomposed density of states (DOS) (Figure 1) that the calculated band gap of NiO_x using DFT methods is 2.73 eV, which is closer to our experimental data. Moreover, total spin-up and spin-down DOS of all systems we studied are asymmetric, and significantly different near the Fermi level. Our spin-polarized calculations revealed the ferromagnetic behavior in NiO_x and Zn-doped NiO_x, which is consistent with the previous work.[40] Figure 1 also shows that Zn-doped NiO_x with a Ni vacancy has the dramatically different electronic states near the Fermi level compared with other systems. It is clear that the introduction of Zn atom in NiO_x induces more electronic states in the Fermi level, and makes it to be a half-metallic ferromagnet. Thus, we speculate that Zn doping in NiO_x can remarkably improve the electronic conductivity.

To investigate the thermodynamic stability of Zn-doped NiO_x, we calculated the formation energies of $Ni_{31}O_{32}$ and $ZnNi_{30}O_{32}$. The formula to calculate formation energies of neutral defects can be expressed as [41]

$$E_f = E_{defect}^{tot} - E_0^{tot} - n_+\mu_+ + n_-\mu_-.$$

E_{defect}^{tot} is the total energy of the supercell with a relaxed defect, and E_0^{tot} is the total energy of the same supercell without defects. n_+ and n_- are the number of atoms added to and removed from the supercell in forming the defect cell, respectively. μ_+ and μ_- are the corresponding energies of the species. For $Ni_{31}O_{32}$, $n_+ = 0, n_- = n_{Ni} = 1$, the calculated formation energy of a Ni vacancy is 0.58 eV, which is in good accordance with the reported values in references.[42] While, for $ZnNi_{30}O_{32}$, $n_+ = n_{Zn} = 1$ and $n_- = n_{Ni} = 2$, the formation energy derived from DFT calculation is -2.64 eV, much smaller than that of $Ni_{31}O_{32}$. These results show that Zn-doped NiO_x is more energetically stable than undoped NiO_x. Thus, the introduction of Zn atoms in NiO_x is favorable for the formation of Ni vacancies and leads to the improvement of the conductivity in NiO_x. Our calculations predict that Zn-doped NiO_x (NiO_x:Zn) with enhanced conductivity could be a good candidate for high efficiency PSCs.

To directly prove our theoretical predictions, we fabricate NiO_x:Zn and NiO_x films by spin-coating method and characterized their morphology and electronic properties. The surface morphologies of NiO_x:Zn and NiO_x films were first studied using scanning electron microscope (SEM). As shown in Figure 2a-b, the NiO_x:Zn film exhibits very compact and continuous morphology without pinholes or crevices in comparison with the NiO_x films. Clearly, the Zn doping enhanced grain growth within the NiO_x film.[43] The atomic force microscope (AFM) was used to further characterize the roughness of the compact NiO_x films as shown in Figure 2c-d. The results demonstrate that Zn-doping results in a gratifying smooth surface with a

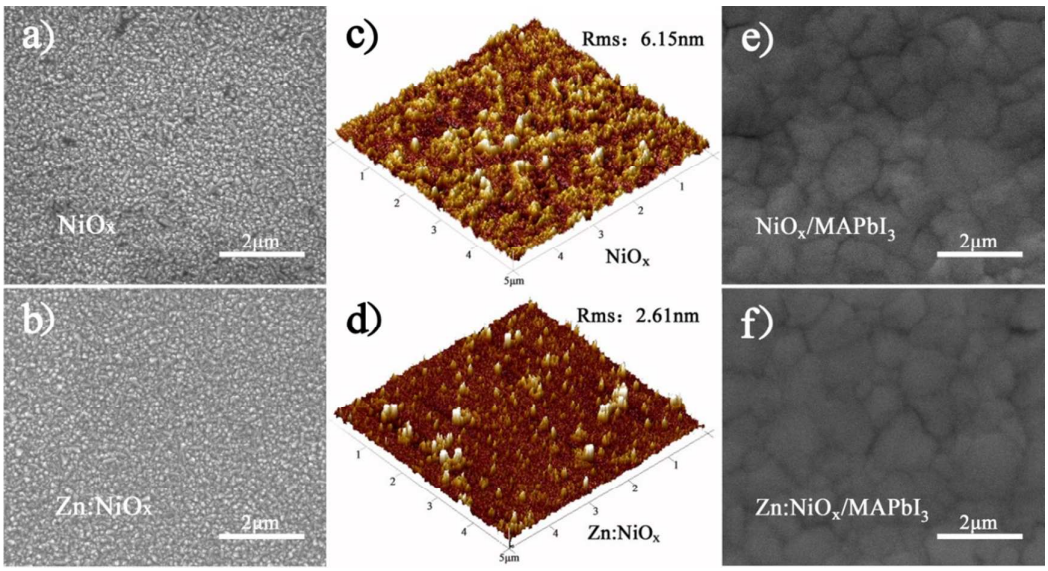

Figure 2. SEM images of a) the NiO_x and b) NiO_x:Zn on FTO glass. 3D AFM images of c) the corresponding NiO_x and d) NiO_x:Zn films. The scan area is 25μm^2 (5 μm × 5 μm). SEM images of perovskite films on e) NiO_x and f) NiO_x:Zn. All scale bars are 2 μm.

smaller root mean square (Rms) surface roughness (2.61 nm) compared to undoped NiO_x film with a Rms of 6.15 nm. Similarly, when such NiO_x:Zn film was employed as hole extraction layers for invert PSC, a continuous, full coverage, and smooth $MAPbI_3$ perovskite film are grown onto such NiO_x:Zn film, which is one desired property for obtaining high efficient perovskite solar cell devices.

Figure 3 shows the X-ray photoelectron spectroscopy (XPS) spectra of Zn 2p and Ni 2p3/2 core level for NiO_x and NiO_x:Zn films. Figure 3a demonstrates that Zn is incorporated into NiO_x:Zn film in its divalent state with an atomic ratio of 4.73% as shown in Table 1 and Figure S1. The Ni 2p3/2 spectra (Figure 3b) can be well fitted with three different states including NiO_x (Ni 2p3/2 at 853.8 eV), Ni_2O_3 (Ni 2p3/2 at 855.3 eV), and satellite peak of Ni^{3+} (Ni 2p3/2 at 856.1 eV). As calculated

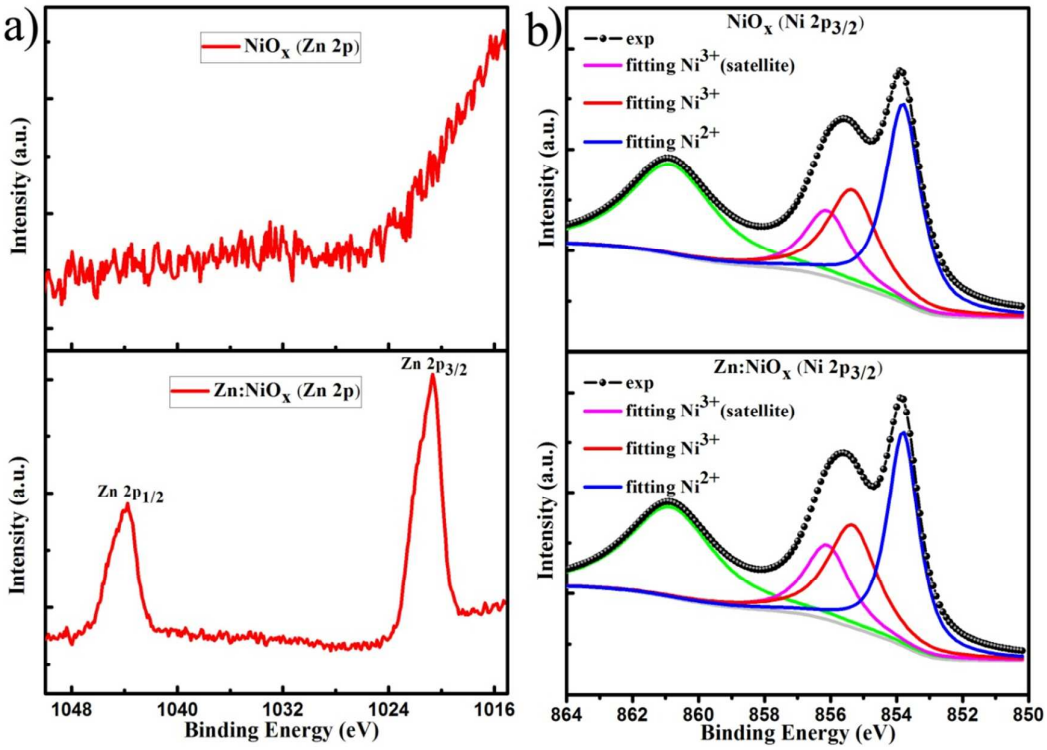

Figure 3. High-resolution XPS spectra of the Zn (a) and Ni (b) elements in NiO_x and NiO_x:Zn films, respectively. After doping, Zn^{2+} signal and increasing Ni^{3+} composition were clearly detected simultaneously.

Table 1 Summary of the Ni, O and Zn Atomic ratio in NiO_x and NiO_x:Zn films respectively.

Sample	Ni (%)	Ni^{3+}/Ni^{2+}	O (%)	Zn (%)	Ni/O ratio	(Ni+Zn)/O ratio
NiO_x	39.36	1.06	44.06	0	0.89	0.89
NiO_x:Zn	34.92	1.27	44.86	4.73 %	0.78	0.86

from the integrated peak area, the Ni^{3+}/Ni^{2+} ratios are obtained to be 1.06 and 1.27 for NiO_x and NiO_x:Zn samples respectively, and we observe a clear increasing Ni^{3+} composition in the Ni 2p spectra of the doped samples. Thus, this indicates more nickel vacancies are produced as a result of Zn doping. NiO_x is also known for its

tendency to contain Ni vacancies (Ni/O:0.89), which is also the defect nature for its intrinsic p-type conductivity.[44] As a typical ionic material, its metallic character often drives substitutional site preference and makes Zn atoms substitute in Ni sites. The improvement of the Ni^{3+}/Ni^{2+} ratio further reveals Zn doping reduces the ionization energy of the Ni vacancies, and thus improving the hole densities, which is in good agreement with our DFT predictions.

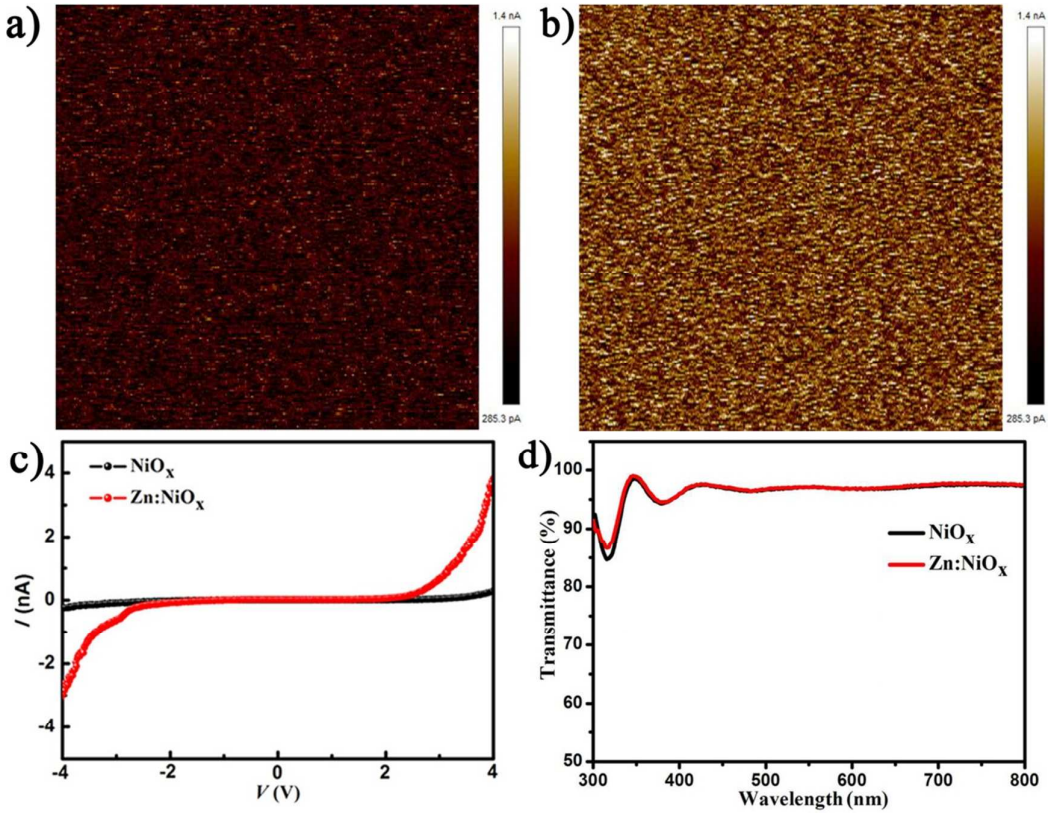

Figure 4. Conductive atomic force microscopy (c-AFM) images of a) the undoped NiO_x film and b) doped NiO_x:Zn film (the scan area is 4 μm x 4 μm); c) I-V conducting curves of the NiO_x and NiO_x:Zn films measured from the c-AFM mode; d) Transmittance spectra of the NiO_x and NiO_x:Zn films coated on glass substrates..

The electrical conductivities of NiO_x and NiO_x:Zn films were investigated by conductive AFM (c-AFM) scanning measurement, as shown in Figure 4a-b. Replacing the undoped NiO_x with doped NiO_x:Zn film can significantly increase the

vertical current, which indicates the better electrical conductivity of NiO_x film after Zn doping. Due to the existence of Schottky barrier potential, the current changes in the range of -2~2 V is minor, as shown in Figure 4c. However, the I-V curves exhibit dramatically enhanced electrical current from 0.25 to 3.9 nA at a bias potential of 4.0 V. The optical property of NiO_x and NiO_x:Zn films is compared in the UV-vis absorption spectra, as shown in Figure 4d. The transmittance of the NiO_x and NiO_x:Zn film express extremely similar transmission spectra and both the films exhibit above 95% transmittance over a broad spectral range from 300 to 800 nm using the bare glass as the reference. Such high transparent substrate and HTM is another reason for achieving high perovskite solar cell PCE.

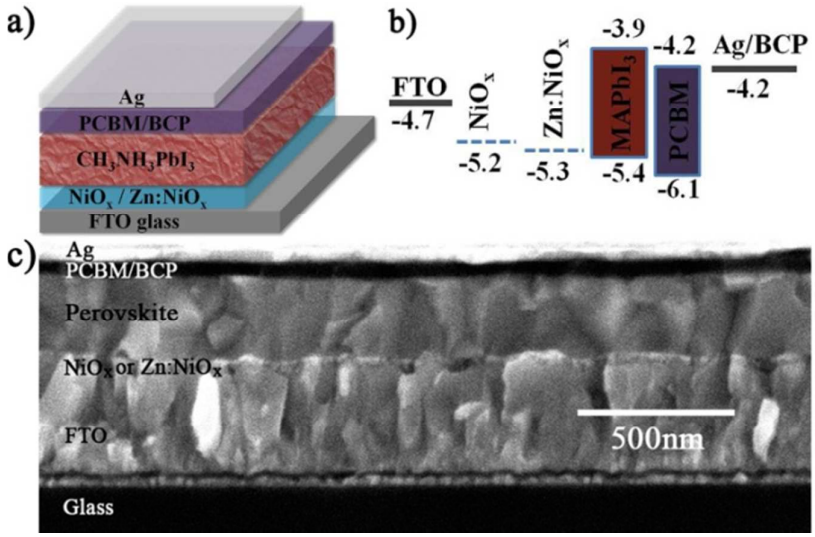

Figure 5. a) Device architecture of the inverted planar perovskite solar cell (PSCs). b) Energy band level diagram of the various layers in the PSCs. c) Cross-section SEM image of a complete perovskite device with NiO_x or NiO_x:Zn film as HTM.

To further prove the influence of NiO_x doping on the PSC performance, PSCs with an P-i-N inverted planar structure of glass/FTO/NiO_x(NiO_x:Zn)/$MAPbI_3$/PCBM/BCP/Ag multi-layers and the

corresponding energy band diagrams are depicted in Figure 5a-b. Figure 5c is a typical cross-sectional SEM image of the PSC device. The NiO_x or Zn doped NiO_x layer was prepared on the top of the glass/FTO substrate by spin-coating NiO_x or NiO_x:Zn precursor solution in glycol (Experimental Section). The $MAPbI_3$ film of 250–300 nm was then prepared by one-step solvent engineering method, as reported by Zhang *et al*.[45] PCBM as ETM was spin-coated on $MAPbI_3$ film with thickness of 30 nm. Thereafter, 15 nm BCP film was adopted as an electrode interface layer to reduce energy barrier for electron transporting. Finally, the Ag cathode was deposited by vacuum vapor deposition to complete the device structure.

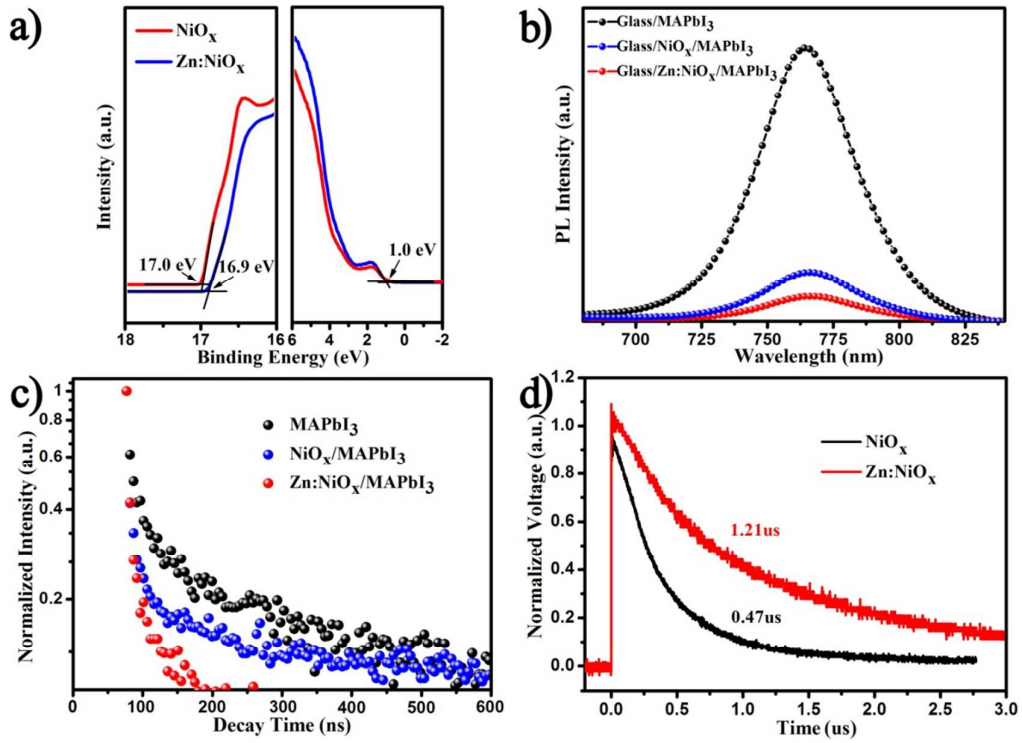

Figure 6. a) The ultraviolet photoelectron spectroscopy (UPS) of the NiO_x and NiO_x:Zn films coated on glass, measured under 21.2 eV bias. b) PL spectra and c) Time-resolved PL spectra for perovskite films on different substrates: glass (black), NiO_x (blue), and NiO_x:Zn (red). d) Transient photovoltage (TPV) as function of time for solar cells with NiO_x and Zn-doped NiO_x film as hole transport interlayers, respectively.

Figure 6a compares the ultraviolet photoelectron spectroscopy (UPS) spectra of the NiO_x with NiO_x:Zn films and the work function of the NiO_x and NiO_x:Zn are calculated by the formula $\Phi = h\nu - (E_0\text{-}E_F)$. The VB spectra were determined with a monochromatic He I light source (21.2 eV)，and the work function (ϕ) can be calculated by the difference between the photon energy and the binding energy of the secondary cutoff edge. NiO_x:Zn doped film has a higher work function, and generates the descending VB from -5.2 eV to -5.3 eV, which is similar to that of $MAPbI_3$ (-5.4 eV). According to the energy level diagram as presented in Figure 5b, the shifted VB makes energy level distribute between NiO_x hole transport layer and perovskite VB, and, therefore, improves hole extraction efficiency tremendously. To verify this inference, photoluminescence properties of different samples were measured in Figure 6b-c. Steady-state photoluminescence (PL, Figure 6b) and time-resolved PL spectra (TRPL, Figure 6c) for perovskite films on glass substrate (black), NiO_x (blue), and NiO_x:Zn (red) films illustrate that the NiO_x:Zn hole transport layer forms a more favorable ohmic contact with perovskite photosensory layers and obviously improves the hole extraction efficiency. Furthermore, the charge-recombination lifetime of the NiO_x:Zn based solar cell device measured by transient photovoltage spectrum (Figure 6d) is 1.21 μs, which is much bigger than that of NiO_x based device (0.47 μs). Longer interfacial recombination lifetime can guarantee effective charge collection efficiency, and, as a result, higher device output photovoltage. Moreover, the improvement of such interfacial engineering can also be attributed to the improved film morphology discussed earlier in Figure 2, and can further decipher the reason for enhancing the

performance of devices.

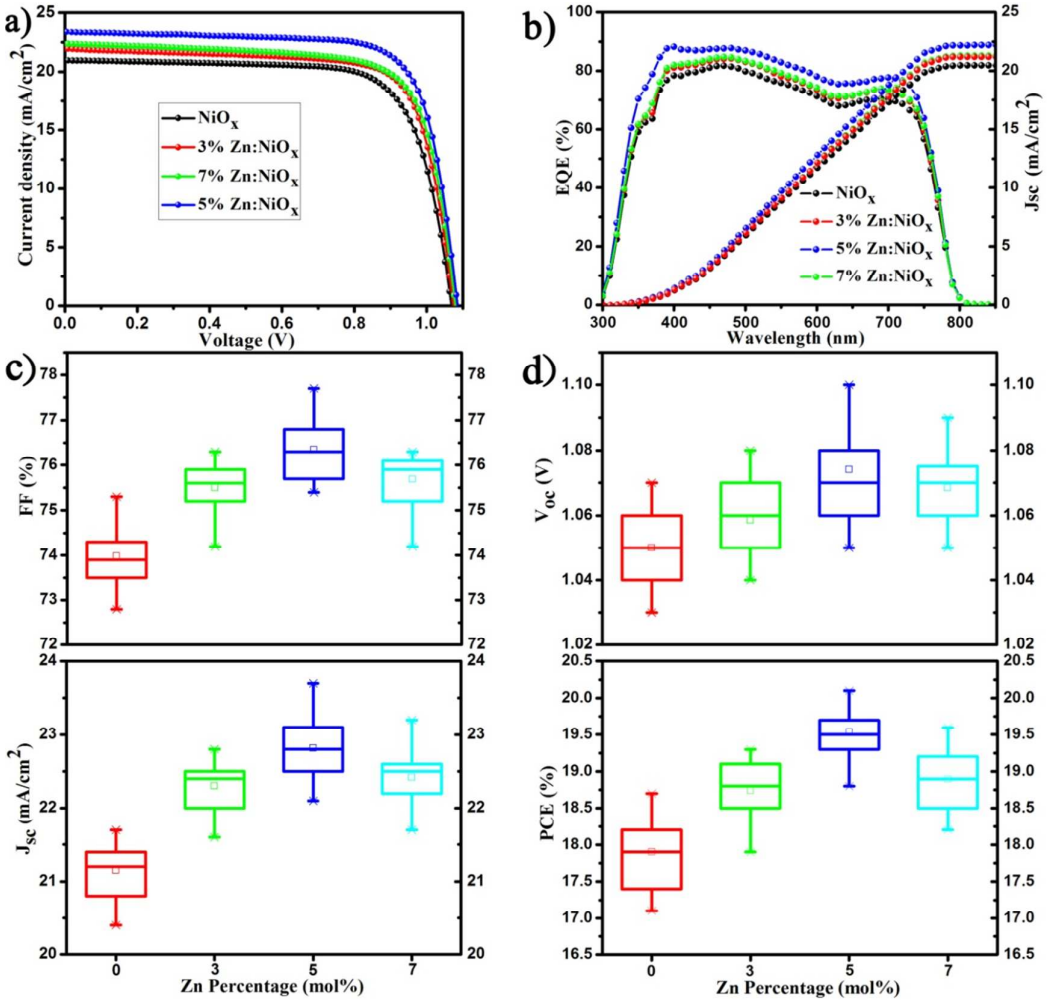

Figure 7. a) I-V curves of the PSCs with NiO_x:Zn HTM of different Zn content in NiO_x:Zn. and b) the corresponding external quantum efficiency spectra with various Zn content in NiO_x:Zn. c,d) Photovoltaic property parameters of the unencapsulated PSCs with different Zn content in NiO_x:Zn.

In order to optimize the Zn dopant concentrations in NiO_x, NiO_x:Zn films were prepared by adding Zn precursors with different molar ratios (3–7 mol%). The current density–voltage (J-V) characteristics of the best devices based on NiO_x:Zn HTL with various amount of Zn dopant are shown in Figure 7a. The corresponding external quantum efficiency (EQE) spectra are also shown in Figure 7b. We can conclude that

adding Zn precursors at 5 mol% molar ratios can gain the best device performance. Therefore, all of the following devices are prepared with this optimized dopant concentration. We compared the photovoltaic (PV) parameters of the PSCs with different HTLs (NiO_x and NiO_x:Zn). In striking contrast, the devices with NiO_x:Zn HTL layer exhibited significantly improved performance with a J_{SC} of 22.8 mA cm^{-2}, V_{OC} of 1.1 V, FF of 78%, and according PCE of 19.6%. Moreover, the obtained photovoltaic performances properties for devices with various Zn contents are summarized in Figure 7c-d, and it shows that the promotion of the efficiency for the device with doped HTL is mainly due to the increasing photocurrent, which is also further confirmed by higher EQE value compared with that of the pristine device with HTL without Zn doping.

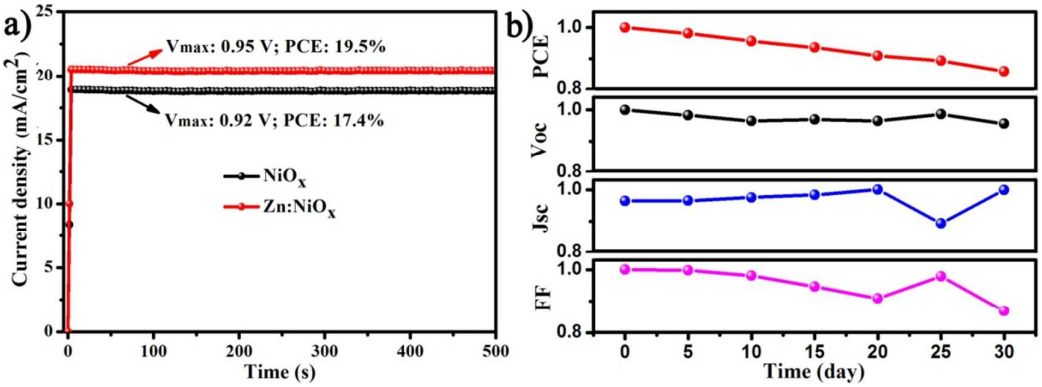

Figure 8. a) Steady-state photocurrent output at the maximum power point of the corresponding cells under continuous simulated AM1.5G light illumination for 500 s. b) Stability of the NiO_x:Zn based devices in a dry environment without encapsulation by measuring the normalized Voc, Jsc, FF, and PCE.

The steady-state photocurrent output at the maximum power point over 500 s has been measured by setting a bias at the maximum power output point (P_{max}, 0.95 V). There is no performance degradation under long illumination and the light current

stabilizes quickly when the light was on, as shown in Figure 8a. The performance enhancement and hysteresis-free behavior were tentatively attributed to the improved hole extraction efficiency. Finally, in order to examine the device stability, we monitored the PV parameters of the unencapsulted devices which were stored in dry air and tested in ambient environment with a relative humidity of 50%~60%. The corresponding photovoltaic performance parameters were measured for over one month, as shown in Figure 8b. Meanwhile, we compared with the pristine NiO_x-based system, and found that the stability of Zn-based system did not change significantly as shown in Figure S2. Finally, we observed a distinguished devices stability that maintained about 85% initial efficient after one month, which is very promising for future development of inverted planar PSCs.

3. Conclusion

In summary, we have successfully demonstrated effective and stable Zn doped NiO_x films as the HTL for inverted planar PSCs and addressed the effects of Zn doping on electronic properties of NiOx HTL and therefore the solar cell device performance. The new Zn dopant could improve the surface morphology and conductivity of NiO_x:Zn film and thereafter significantly enhance the photon conversion efficiency of P-i-N planar PSC using NiO_x:Zn as HTL. The best-performing device exhibited a remarkable efficiency of 19.6% with negligible hysteresis and a praiseworthy stability over long time, which is a promising candidate for future development of inverted planar PSCs.

ASSOCIATED CONTENT

Supporting Information

The Supporting Information is available free of charge on the ACS Publications website at DOI: .

Experimental Section; XPS from NiO_x film and NiO_x:Zn film respectively; Stability of the NiO_x based devices in a dry environment without encapsulation

The authors declare no competing financial interest.

AUTHOR INFORMATION

Corresponding Author

* Prof. Bingqiang Cao, mse_caobq@ujn.edu.cn.

* Prof. Xin Chen, chenxin@qfnu.edu.cn

Acknowledgment

This work is supported by National Natural Science Foundation of China (NSFC 51472110) and Shandong Provincial Natural Science Foundation (ZR2017ZB0316).

References

(1) Yang, W. S.; Park, B.-W.; Jung, E. H.; Jeon, N. J.; Kim, Y. C.; Lee, D. U.; Shin, S. S.; Seo, J.; Kim, E. K.; Noh, J. H.; Seok, S. I. Iodide Management in Formamidinium-Lead-Halide-based Perovskite Layers for Efficient Solar Cells. *Science.* **2017**, *356*, 1376-1379.

(2) Jang, S.; Yoon, J. ; Ha, K.; Kim, M.-C.; Kim, D.H. ; Kim, S.M. ; Kang, S.M.; Park, S.J.; Jung, H.S.; Choi, M. Facile Fabrication of Three-Dimensional TiO_2 Structures for Highly Efficient Perovskite Solar Cells. *Nano Energy.* **2016**, *22*, 499-506.

(3) Stranks, S. D.; Eperon, G. E.; Grancini, G.; Menelaou, C.; Alcocer, M. J. P.; Leijtens, T.; Herz, L. M.; Petrozza, A.; Snaith, H. J. Electron-Hole Diffusion Lengths Exceeding 1 Micrometer in an Organometal Trihalide Perovskite Absorber. *Science.* **2013**, *342*, 341-344.

(4) Xing, G. C.; Mathews, N.; Sun, S. G.; Lim, S. S.; Lam, Y. M.; Grätzel, M.; Mhaisalkar, S.; Sum, T. C. Long-Range Balanced Electron-and Hole-Transport

Lengths in Organic-Inorganic $CH_3NH_3PbI_3$. *Science.* **2013**, *342*, 344-347.

(5) Park, I. J.; Park, M. A.; Kim, D. H.; Park, G. D.; Kim, B. J.; Son, H. J.; Ko, M. J.; Lee, D.-K.; Park, T.; Shin, H.; Park, N.-G.; Jung, H. S.; Kim, J. Y. New Hybrid Hole Extraction Layer of Perovskite Solar Cells with a Planar P-i-N Geometry. *J. Phys. Chem. C.* **2015**, *119*, 27285-27290.

(6) Leijtens, T.; Stranks, S. D.; Eperon, G. E.; Lindblad, R.; Johansson, E. M. J.; McPherson, I. J.; Rensmo, H.; Ball, J. M.; Lee, M. M.; Snaith, H. J. Electronic Properties of Meso-Superstructured and Planar Organometal Halide Perovskite Films: Charge Trapping, Photodoping, and Carrier Mobility. *ACS Nano.* **2014**, *8*, 7147-7155.

(7) Kim, M.-C.; Kim, B. J.; Yoon, J.; Lee, J.-W.; Suh, D.; Park, N.-G.; Choi, M.; Jung, H. S. Electro-Spray Deposition of a Mesoporous TiO_2 Charge Collection Layer: Toward Large Scale and Continuous Production of High Efficiency Perovskite Solar Cells. *Nanoscale.* **2015**, *7*, 20725-20733.

(8) Zuo, C.; Bolink , H. J.; Han, H.; Huang, J.; Cahen, D.; Ding, L. Advances in Perovskite Solar Cells. *Adv. Sci.* **2016**, *3*, 7.

(9) Yan, W. B.; Ye, S. Y.; Li, Y. L.; Sun, W. H.; Rao, H. X.; Liu, Z. W.; Bian, Z. Q.; Huang, C. Hole-Transporting Materials in Inverted Planar Perovskite Solar Cells. *Adv. Energy Mater.* **2016**, *6*, 100-108.

(10) Li, M.-H.; Shen, P.-S.; Wang, K.-C.; Guo, T.-F.; Chen, P. Inorganic P-Type Contact M aterials for Perovskite-Based Solar Cells. *J. Mater. Chem. A.* **2015**, *3*, 9011-9019.

(11) Liu, Y.; Renna, L. A.; Page, Z. A.; Thompson, H. B.; Kim, P. Y.; Barnes, M. D.; Emrick, T.; Venkataraman, D.; Russell, T. P. A Polymer Hole Extraction Layer for Inverted Perovskite Solar Cells from Aqueous Solutions. *Adv. Energy Mater.* **2016**, *6*, 1600664.

(12) Zhao, D.; Sexton, M.; Park, H.-Y.; Baure, G.; Nino, J. C.; So, F. High-Efficiency Solution-Processed Planar Perovskite Solar Cells with a Polymer Hole Transport Layer. *Adv. Energy Mater.* **2015**, *5*, 1401855.

(13) Jung, J. W.; Chueh, C. C.; Jen, A. K.-Y. High-Performance Semitransparent

Perovskite Solar Cells with 10% Power Conversion Efficiency and 25% Average Visible Transmittance Based on Transparent. *Adv. Mater.* **2015**, *5*, 7874-7880.

(14) You, J.; Yang, Y.; Hong, Z.; Song, T.-B.; Meng, L.; Liu, Y.; Jiang, C.; Zhou, H.; Chang, W.-H.; Li, G.; Yang, Y. Moisture Assisted Perovskite Film Growth for High Performance Solar Cells. *Appl. Phys. Lett.* **2014**, *105*, 183902.

(15) Sun, S.; Salim, T.; Mathews, N.; Duchamp, M.; Boothroyd, C.; Xing, G.; Sumbce, T. C.; Lam, Y. M. The Origin of High Efficiency in Low-Temperature Solution-Processable Bilayer Organometal Halide Hybrid Solar Cells. *Energy Environ. Sci*. **2013**, *7*, 399-407.

(16) Zheng, X.; Chen, B.; Dai, J.; Fang, Y.; Bai, Y.; Lin, Y.; Wei, H.; Zeng, X. C.; Huang, J. Defect Passivation in Hybrid Perovskite Solar Cells Using Quaternary Ammonium Halide Anions and Cations. *Nat. Energy.* **2017**, *2*, 17102.

(17) Zhou, H.; Zhou, Q.; Li, G.; Luo, S.; Song, T. B.; Duan, H. S.; Hong, Z.; You, J.; Liu, Y.; Yang, Y. Interface Engineering of Highly Efficient Perovskite Solar Cells. *Science.* **2014**, *345*, 542-546.

(18) Luo, Q.; Zhang, Y.; Liu, C.; Li, J.; Wang, N.; Lin, H. IodideReduced Graphene Oxide with Dopant-Free spiro-OMeTAD for Ambient Stable and High-Efficiency Perovskite Solar Cells. *J. Mater. Chem. A.* **2015**, *3*, 15996-16004.

(19) Luo, Q.; Ma, H.; Zhang, Y.; Yin, X.; Yao, Z.; Wang, N.; Li, J.; Jiang, K.; Lin, H. Cross-Stacked Superaligned Carbon Nanotube Electrode for Efficient Hole Conductor-Free Perovskite Solar Cells. *J. Mater. Chem. A.* **2016**, *4*, 5569-5577.

(20) Zhang, Y.; Liu, M.; Eperon, G. E.; Leijtens, T. C.; McMeekin, D.; Saliba, M.; Zhang, W.; Bastiani, M.; Petrozza, A.; Herz, L. M.; Johnston, M. B.; Lin, H.; Snaith, H. J. Charge Selective Contacts, Mobile Ions and Anomalous Hysteresis in Organic-Inorganic Perovskite Solar Cells. *Mater. Horiz.* **2015**, *2*, 315-322.

(21) Qin, P.; Tanaka, S.; Ito, S.; Tetreault, N.; Manabe, K.; Nishino, H.; Nazeeruddin, M. K.; Grätzel, M. Inorganic Hole Conductor-Based Lead Halide Perovskite Solar Cells with 12.4% Conversion Efficiency. *Nat. Commun.* **2014**, *5*, 1-6.

(22) Subbiah, A. S.; Halder, A.; Ghosh, S.; Mahuli, N.; Hodes, G.; Sarkar, S. K. Inorganic Hole Conducting Layers for Perovskite-Based Solar Cells. *J. Phys.*

Chem. Lett.. **2014**, *5*, 1748-1753.

(23) Christians, J. A.; Fung, R. C. M.; Kamat, P. V. An Inorganic Hole Conductor for Organo-Lead Halide Perovskite Solar Cells: Improved Hole Conductivity with Copper Iodide. *J. Am. Chem. Soc.* **2014**, *136*, 758-764.

(24) Zuo, C.; Ding, L. Solution-Processed Cu_2O and CuO as Hole Transport Materials for Efficient Perovskite Solar Cells. *Small.* **2015**, *11*, 5528-5532.

(25) Xu, X. B.; Liu, Z. H.; Zuo, Z. X.; Zhang, M.; Zhao, Z. X.; Shen, Y.; Zhou, H. P.; Chen, Q.; Yang, Y.; Wang, M. K. Hole Selective NiO Contact for Efficient Perovskite Solar Cells with Carbon Electrode. *Nano Lett.* **2015**, *15*, 2402-2408.

(26) Jeng, J.-Y.; Chiang, Y.-F.; Lee, M.-H.; Peng, S.-R.; Guo, T.-F.; Chen, P.; Wen, T.-C. $CH_3NH_3PbI_3$ Perovskite/Fullerene Planar-Heterojunction Hybrid Solar Cells. *Adv. Mater*. **2013**, *25*, 3727-3732.

(27) Jeng, J.-Y.; Chen, K.-C.; Chiang, T.-Y.; Lin, P.-Y.; Tsai, T.-D.; Chang, Y.-C.; Guo, T.-F.; Chen, P.; Wen, T.-C.; Hsu, Y.-J. Nickel Oxide Electrode Interlayer in $CH_3NH_3PbI_3$ Perovskite/PCBM Planar-Heterojunction Hybrid Solar Cells. *Adv. Mater*. **2014,** *26*, 4107-4113.

(28) Hu, L.; Peng, J.; Wang, W. W.; X, Z.; Yuan, J.; Lu, J. L.; Huang, X. D.; Ma, W. L.; Song, H. B.; Chen, W.; Cheng, Y. B.; Tang, J. The Growth of a $CH_3NH_3PbI_3$ Thin Film using Simplified Close Space Sublimation for Efficient and Large Dimensional Perovskite Solar Cells. *ACS Photonics.* **2014**, *1*, 547-553.

(29) Kim, J. H.; Liang, P. W.; Williams, S. T.; Cho, N.; Chueh, C.-C.; Glaz, M. S.; Ginger, D. S.; Jen, A. K.-Y. High-Performance and Environmentally Stable Planar Heterojunction Perovskite Solar Cells Based on a Solution-Processed Copper-Doped Nickel Oxide Hole. *Adv. Mater.* **2015**, *27*, 695-701.

(30) Irwin, M. D.; Buchholz, B.; Hains, A. W.; Chang, R. P. H.; Marks, T. J. P-Type Semiconducting Nickel Oxide as an Efficiency-Enhancing Anode Interfacial Layer in Polymer Bulk-Heterojunction Solar Cells. *Proc. Natl. Acad. Sci. USA* **2008**, *105*, 2783-2787.

(31) Manders, J. R.; Tsang, S.-W.; Hartel, M. J.; Lai, T.-H.; Chen, S.; Amb, C. M.; Reynolds, J. R.; So, F. Solution-Processed Nickel Oxide Hole Transport Layers

in High Efficiency Polymer Photovoltaic Cells. *Adv. Funct. Mater.* **2013**, *23*,2993-3001.

(32) Corani, A.; Li, M.-H.; Shen, P.-S.; Chen, P.; Guo, T.-F.; Nahhas, A. E.; Zheng, K.; Yartsev, A.; Sundström, V.; Ponseca, C. S. Ultrafast Dynamics of Hole Injection and Recombination in Organometal Halide Perovskite Using Nickel Oxide as P-Type Contact Electrode. *J. Phys. Chem. Lett.* **2016**, *7*, 1096-1101.

(33) Wu, C. C.; Shih, W. C. Development of a Highly Transparent, Low-Resistance Lithium-Doped Nickel Oxide Triple-Layer Film Deposited by Magnetron Sputtering. *Chem. Commun.* **2017**, *53*, 1634-1637.

(34) Kim, J.; Lee, H. R.; Kim, H. P.; Lin, T.; Kanwat, A.; Yusoffa, A. R. M.; Jang, J. Effects of Cu Doping on Nickel Oxide Thin Film Prepared by Sol-Gel Solution Process. *Nanoscale.* **2016**, *8*, 9284-9292.

(35) Datta, T.; Gupta, P.; Gupta, A.; Narayan, J. Effect of Li Doping in NiO Thin Films on Its Transparent and Conducting Properties and Its Application in Heteroepitaxial PN Junctions. *J. Appl. Phys.* **2010**, *108*, 083715.

(36) Fernández, R.; Estelle, J.; Cesteros, Y.; Salagre, P.; Medina, F.; Sueiras, J.-E.; Fierroc, J.-L. G. Structural Characterization of NiO Doped with Several Caesium Loadings. *J. Mol. Catal A:Chem.* **1997**, *119*, 77-85.

(37) Yao, K.; Li, F.; He, Q.; Wang, X.; Jiang, Y.; Huang, H.; Jen, A. K. Y. A Copper-Doped Nickel Oxide Bilayer for Enhancing Efficiency and Stability of Hysteresis-Free Inverted Mesoporous Perovskite Solar Cells. *Nano Energy*, **2017**, *40*, 155-162.

(38) Qiu, Z.; Gong, H.; Zheng, G.; Yuan, S.; Zhang, H.; Zhu, X.; Zhou, H.; Cao, B. Enhanced Physical Properties of Pulsed Laser Deposited NiO Films Via Annealing and Lithium Doping for Improving Perovskite Solar Cell Efficiency. *J. Mater. Chem. C.* **2017**, *5*, 7084-7094.

(39) Chen, W.; Liu, F.-Z.; Feng, X.-Y.; Djurišić, A. B.; Chan, W. K.; He, Z.-B. Cesium Doped NiO_x as an Efficient Hole Extraction Layer for Inverted Planar Perovskite Solar Cells. *Adv. Energy Mater.* **2017**, *7*, 19.

(40) Blöchl, P. E. Projector Augmented-Wave Method. *Phys. Rev. B* **1994**, *50*, 17953.

(41) Wu, R. Q.; Peng, G. W.; Liu, L.; Feng, Y. P.; Huang, Z. G.; Wu, Q. Y. Ferromagnetism in Mg-Doped AlN From Ab Initio Study. *Appl. Phys. Lett.* **2006**, *89*, 142501.

(42) Stephan, L.; Jorge, O.-G.; Alex, Z. Origins of The Doping Asymmetry in Oxides: Hole Doping in NiO Versus Electron Doping in ZnO. *Phys. ReV. B.* **2007**, *75*, 241203.

(43) Bang, K.; Son, G.-C.; Son, M.; Jun, J.-H.; An, H.; Baik, K. H.; Myoung, J.-M.; Ham, M.-H. Effects of Li Doping on The Structural and Electrical Properties of Solution-Processed ZnO Films for High-Performance Thin-Film Transistors. *J. Alloys compd.* **2017**, *739*, 41-46.

(44) Kim, J. H.; Liang, P.-W.; Williams, S. T.; Cho, N.; Chueh, C.-C.; Glaz, M. S.; Ginger, D. S.; Jen, A K.-Y. High-Performance and Environmentally Stable Planar Heterojunction Perovskite Solar Cells Based on a Solution-Processed Copper-Doped Nickel Oxide Hole-Transporting Layer. *Adv. Mater.* **2015**, *27*, 695-701.

(45) Zhang, X.; Yuan, S.; Lu, H.; Zhang, H.; Wang, P.; Cui, X.; Zhang, Y.; Liu, Q.; Wang, J.; Zhan, Y.; Sun, Z.; Huang, W. Hydrazinium Salt as Additive To Improve Film Morphology and Carrier Lifetime for High-Efficiency Planar-Heterojunction Perovskite Solar Cells via One-Step Method. *ACS Appl. Mat. Interfaces.* **2017**, *9*, 36810-36816.

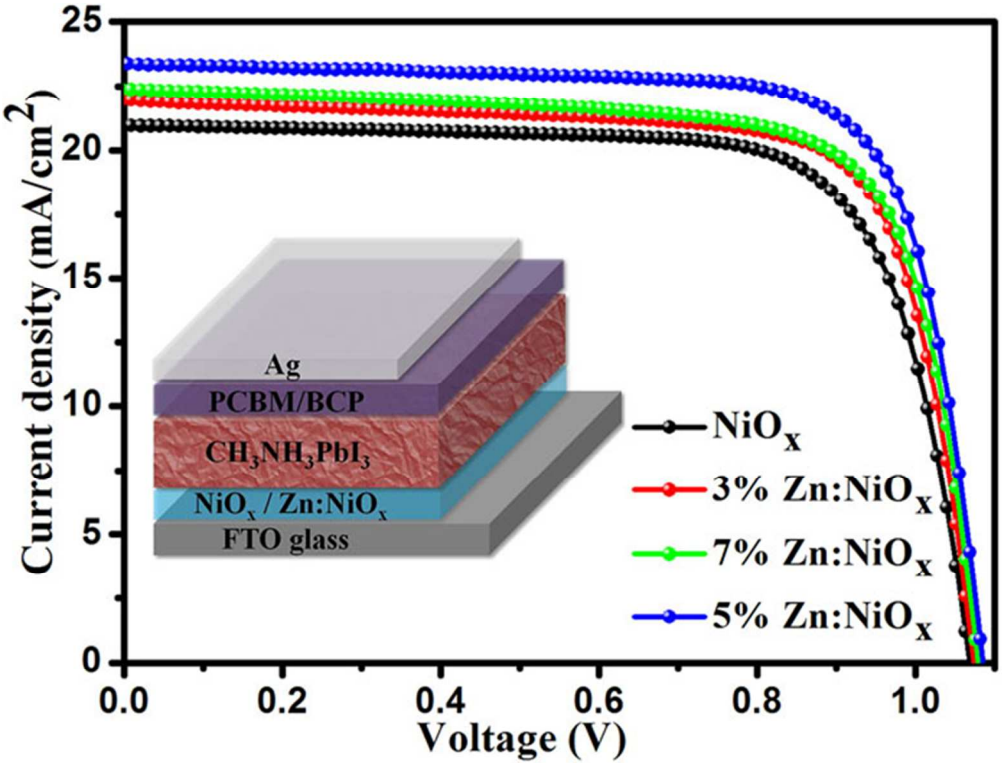

58x44mm (300 x 300 DPI)